Probing the edge of the West African Craton: A first seismic glimpse from Niger

Jeanette F. Di Leo[1], James Wookey[1], J.-Michael Kendall[1], and Neil D. Selby[2]

[1]School of Earth Sciences, University of Bristol, Bristol, UK, [2]AWE Blacknest, Reading, UK

Abstract Constraints on crustal and mantle structure of the Eastern part of the West African Craton have to date been scarce. Here we present results of P receiver function and $SK(K)S$ wave splitting analyses of data recorded at International Monitoring System array TORD in SW Niger. Despite lacking in lateral coverage, our measurements sharply constrain crustal thickness ($\sim$41 km), V_P/V_S ratio (1.69 $\pm$ 0.03), mantle transition zone (MTZ) thickness ($\sim$247 km), and a midlithospheric discontinuity at $\sim$67 km depth. Splitting delay times are low with an average of 0.63 $\pm$ 0.01 s. Fast directions follow the regional surface geological trend with an average of 57 $\pm$ 1°. We suggest that splitting is due to fossil anisotropic fabrics in the crust and lithosphere, incurred during the Paleoproterozoic Eburnean Orogeny, with possible contributions from the later Pan-African Orogeny and present-day mantle flow. The MTZ appears to be unperturbed, despite the proximity of the sampled region to the deep cratonic root.

1. Introduction

The African continent is an amalgam of some of the oldest continental terranes and cratons, such as the Kalahari, the Tanzania, the Congo, and the West African craton, which were consolidated mainly during the Pan-African Orogeny ($\sim$600–500 Ma) (Figure 1) [e.g., *Van Hinsbergen et al.*, 2011, and references therein]. Multiple mountain belts across the continent bear evidence of these events as extreme examples of surface topography. Topography is arguably the most basic property of the Earth's surface but has wide-ranging consequences for a variety of processes (e.g., weathering and erosion or atmospheric circulation). In order to quantify the effect mantle dynamics have on exospheric processes (i.e., dynamic topography) [*Braun*, 2010], it is crucial to have accurate constraints on crustal and lithospheric thickness and composition, parameters required for removing the isostatic component of the topography. Furthermore, an understanding of the local and/or global mantle flow field is essential.

Both receiver function (RF) and shear wave splitting analyses are routinely used to study the Earth's structure and dynamics. P wave RFs are generated by deconvolving the P wave arrival (recorded on the vertical component) from the horizontal components to reveal P-to-S conversions from velocity discontinuities beneath the station, such as the Moho [*Langston*, 1979] or the 410 and 660 km discontinuities bounding the mantle transition zone (MTZ) [e.g., *Gurrola et al.*, 1994]. Unlike S-to-P RFs, P RFs generally cannot resolve the lithosphere-asthenosphere boundary (LAB), as crustal reverberations mask arrivals from boundaries at depths of $\sim$100–200 km. However, midlithospheric discontinuities (MLD) have frequently been detected in cratons using either P or S RFs [e.g., *Snyder*, 2008; *Abt et al.*, 2010; *Miller and Eaton*, 2010; *Snyder et al.*, 2013; *Cooper and Miller*, 2014]. These MLDs are likely to stem from the formation of the cratons. For example, if they formed through thrust stacking of buoyant material, the resulting localized shear zones may be preserved as fossil anisotropic fabrics. If, however, cratons formed by viscous thickening of buoyant material, it is possible that seismically observable compositional variations developed at depth. Being the most tectonically stable regions on Earth, cratons may retain deformational features (e.g., MLDs) incurred during their formation that can prevail over billions of years. RFs can thus help shed light on the evolution of cratons.

In addition to that, constraints on MTZ thickness may yield insights about subcratonic mantle temperature conditions. Previous workers have argued that deep cratonic roots might cause temperature perturbations in the surrounding mantle; however, while some believe this leads to cooling, others argue it leads to heating [*Thompson et al.*, 2011, and references therein]. Both heating and cooling would result in small-scale convective flow around the cratonic keel, which may be observed seismically [e.g., *King and Ritsema*, 2000].
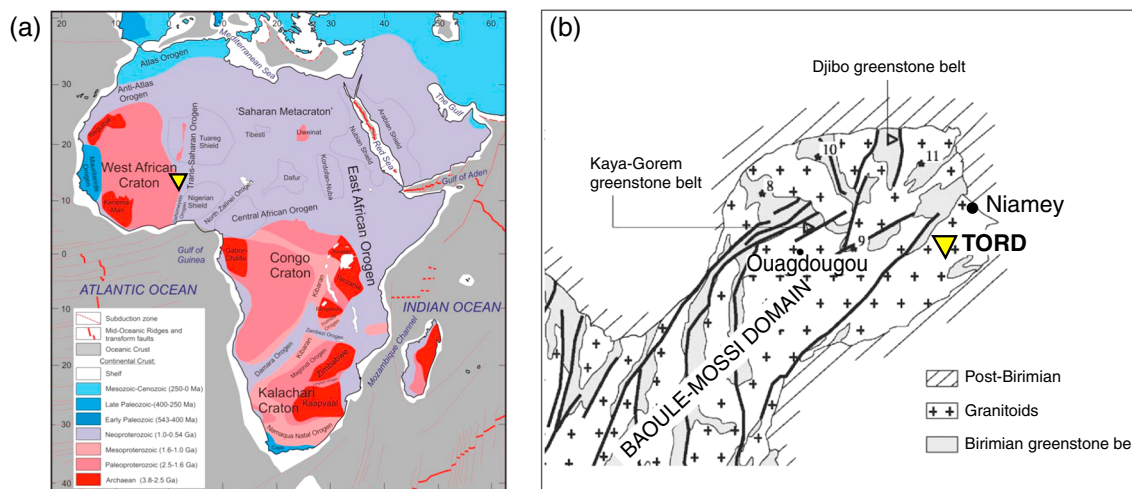
Figure 1. Simplified geological maps by (a) *Van Hinsbergen et al.* [2011] and (b) *Debat et al.* [2003]. Yellow inverted triangle marks the location of the TORD array.

Due to the nature of the two MTZ discontinuities' Clapeyron slopes, significantly decreased or elevated temperatures would be reflected in a MTZ that is either thicker or thinner, respectively, than the global average thickness [*Helffrich*, 2000].

Seismic anisotropy, the directional dependence of seismic wave speed, may be caused by various mechanisms, such as strain-induced lattice-preferred orientation of mantle minerals [e.g., *Hess*, 1964; *Nicolas and Christensen*, 1987] or shape-preferred orientation features in the crust and lithosphere, e.g., aligned fractures or melt [e.g., *Mainprice and Nicolas*, 1989]. Seismic anisotropy can give rise to shear wave splitting, which we measure as the orientation of the fast shear wave (ϕ) and the time lag (δt) between the fast and the slow shear wave. Although placing accurate causal and spatial constraints on anisotropic fabrics is challenging, shear wave splitting observations can potentially provide information on subsurface structure as well as present-day mantle dynamics.

The West African Craton (WAC) is understudied in these respects. Recent observations of its crustal and mantle structure and dynamics mainly come from the NW edge in Morocco [e.g., *Miller et al.*, 2013] or the SE [*Cooper and Miller*, 2014]. Here we add new measurements from the central Eastern region in SW Niger.

2. Data and Methods

In order to determine structural properties of the crust and mantle beneath SW Niger, we employ two well-established teleseismic methods: *P* wave receiver function analysis and $SK(K)S$ shear wave splitting.

We have analyzed data from the Preparatory Commission of the Comprehensive Test Ban Treaty Organization (CTBTO) International Monitoring System (IMS) seismic array TORD, recorded from 2005 to 2013. The 6 km aperture array is located near Torodi, SW Niger, and consists of 16 instruments in total, but due to the nature of our methods, we only analyze data from the 4 three-component broadband sensors.

In preparation for analysis, sensor (horizontal) misorientation analysis was performed using principal component analysis of the particle motion (on the horizontal components) of the *P* wave arrivals of on average 220 events at each station. The weighted (by signal-to-noise ratio) average of the difference between the particle motion direction and the event back azimuth forms the estimate of the misorientation of the horizontal components of the instrument. The variation with time of this misfit was considered; in all but two cases the misorientations did not change over the period of the experiment. TOC4 and TOC6 showed one and two (respectively) definite, abrupt changes of orientation. In all cases the data were corrected using the appropriate measured orientation before further analysis.

2.1. Receiver Functions

Of the 538 earthquakes of magnitude $m_b \geq 5.0$ and an epicentral distance of 30–90°, 269 yielded good-quality RFs (i.e., with a clear *P* onset and a high signal-to-noise ratio). In total, we computed 834 good-quality RFs for the four broadband stations. A high-pass filter of 0.018 Hz was applied with a 0.8 Hz
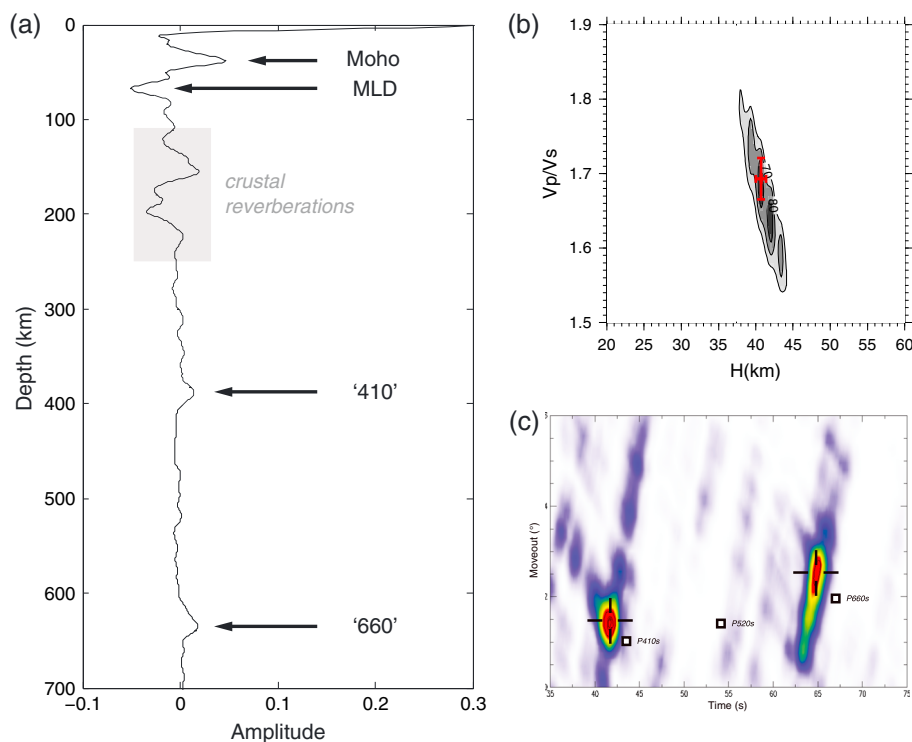
Figure 2. (a) Stacked and depth-migrated receiver functions. Arrows and labels mark pulses from the Moho, a midlitho-spheric discontinuity (MLD), the upper (410) and lower (660) mantle transition zone discontinuities. (b) Crustal thickness (*H*) and V_P/V_S ratio (*H–κ*-stacking after *Zhu and Kanamori* [2000]). (c) Slant-stack of RFs. White squares mark expected time and moveout (traveltime divided by horizontal slowness) of P410s, P520s, and P660s conversions (following *Helffrich et al.* [2003]). P410s and P660s are clearly observed. P520s, however, is not seen at all. Both P410s and P660s arrive early and have a higher moveout than expected, which is due to the lithosphere and mantle being extremely fast in and beneath the WAC [*Becker and Boschi*, 2002]. This, however, has no effect on the MTZ thickness (∼247 km), which is in excellent agreement with the global mean determined by *Lawrence and Shearer* [2006] and *Tauzin et al.* [2008].

cutoff frequency while calculating the receiver functions (following *Helffrich* [2006]). The method we employ is the Extended-Time Multitaper Frequency Domain Cross-Correlation Receiver Function Estimation of *Helffrich* [2006]. Crustal thickness (*H*) and V_P/V_S ratio (*κ*) are determined using the *H-κ* stacking technique of *Zhu and Kanamori* [2000], which stacks amplitudes along predicted moveout curves for the Moho *P*-to-*S*
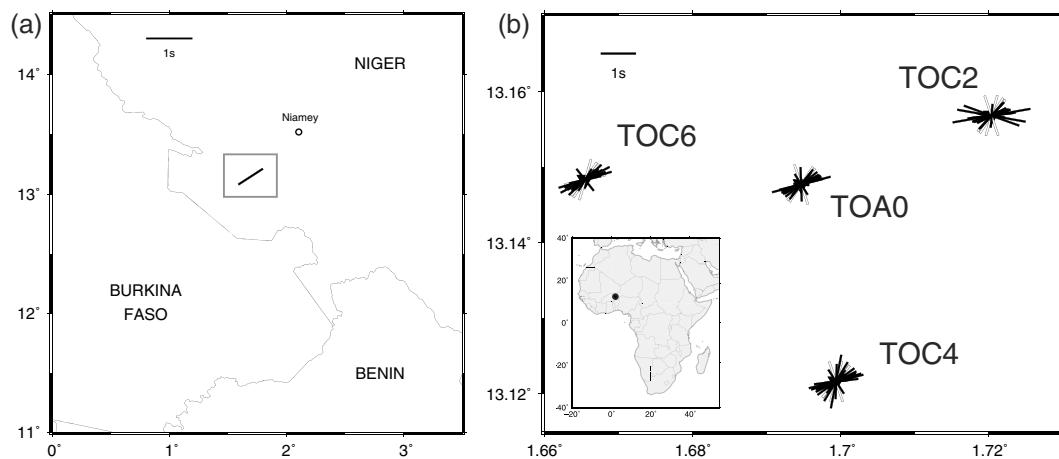
Figure 3. Shear wave splitting results for SW Niger. Bars are oriented in the fast direction, their length is proportional to the delay time. (a) Stacked average of the four stations' splitting measurements. Gray box is the area zoomed into in Figure 3b. (b) Splitting results of individual stations. White bars are null measurements. Inset: black circle marks the study area.

DI LEO ET AL.   1696
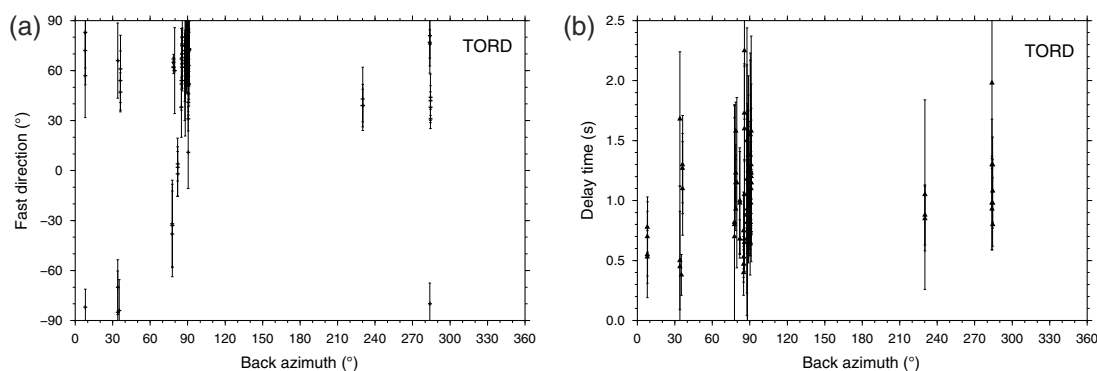
Figure 4. Splitting parameters, (a) fast direction and (b) delay time, versus back azimuth.

conversion and crustal reverberations. We further perform a 1-D common conversion point migration (using the ak135 Earth model of *Kennett et al.* [1995]) of all receiver functions and produce a single summary trace (Figure 2) by linearly stacking the migrated RFs, in order to detect deeper discontinuities, either within the lithosphere or bounding the MTZ.

2.2. Shear Wave Splitting

Of the 383 $SK(K)S$ events of magnitude $m_b \geq 5.0$ and an epicentral distance of 85–140°, 93 events yielded good-quality results: 77 non-null and 16 null measurements (Figure 3). Data were band-pass filtered between 0.03 and 0.4 Hz. We follow the method of *Silver and Chan* [1991] and *Wüstefeld et al.* [2010] to estimate shear wave splitting: a grid search over ϕ and δt determines the parameter pair that minimizes the second eigenvalue of the covariance matrix for the particle motion and thereby corrects for the splitting.

3. Results

Figure 2 shows a 1-D common conversion point depth-migrated stack of all RFs. The prominent *Ps* signal from the Moho is clearly visible. $H - \kappa$ stacking, following the method of *Zhu and Kanamori* [2000], yields a Moho depth of 41.0 ± 0.7 km and a V_P/V_S ratio of 1.69 ± 0.03. The prominent negative conversion at ~67 km depth bears evidence of a midlithospheric discontinuity (MLD), as it is too shallow for it to be the LAB. $P_{410}s$ and $P_{660}s$, marking the bounding discontinuities of the MTZ, are clearly observable. The estimated thickness of the MTZ is ~247 km (Figure 2), which is, in fact, the global mean value determined by *Lawrence and Shearer* [2006] and *Tauzin et al.* [2008]. We detect no azimuthal variability for any of the discontinuities, which suggests that they are all horizontal.

Shear wave splitting results are shown in Figure 3 and listed in Table S1. Fast directions show a clear NE-SW trend with a stacked average [*Wolfe and Silver*, 1998] of 57.00±1.00°. With a stacked average of 0.63 ± 0.01 s, delay times are comparable to those observed in some cratons (e.g., in the Canadian Shield) [*Rondenay et al.*, 2000; *Frederiksen et al.*, 2007]; however, higher delay times have also been observed [e.g., *Kay et al.*, 1999; *Snyder*, 2008; *Snyder et al.*, 2013]. There is no clear variation in splitting parameters with back azimuth, which suggests the presence a single layer of anisotropy (Figure 4).

4. Discussion and Conclusions

4.1. The Crust and Moho

The high-frequency *Ps* arrival (Figure 2) indicates a sharp and flat Moho beneath the array. Furthermore, the crust appears to be seismically transparent, as there is no coherent seismic energy before the Moho *Ps* arrival. TORD sensors were installed in 50 m boreholes in Paleoproterozoic (2.1–2.0 Ga) granodiorite-tonalite, yet the broader surrounding region displays a granitoid-and-greenstone lithology [*Feybesse and Milési*, 1994; *Debat et al.*, 2003]. The low V_P/V_S ratio of 1.69 ± 0.03 we measure is, within error, consistent with the value expected for pure granodiorite [*Christensen*, 1996]. This suggests that a felsic-to-intermediate bulk composition is pervasive throughout the crust, at least beneath our array. The surrounding, interspersed greenstone belts do not appear to have a significant effect, as that would result in a higher V_P/V_S ratio [e.g., *Thompson et al.*, 2010]. Furthermore, the extremely low V_P/V_S ratio rules out a mafic basal crustal layer, an observation that is more reminiscent of Archean than Proterozoic crust [*Durrheim and Mooney*, 1991;

Thompson et al., 2010]. A plausible explanation is that the crust in the study area is, in fact, Archean crust with a tonalite-trondhjemite-granodiorite composition that was reworked during the Eburnean Orogeny (2.1–2.0 Ga), as suggested by *Begg et al.* [2009].

4.2. The Lithosphere

SK(K)S splitting fast directions show a clear ENE-WSW pattern, which is parallel to the surface geological trend and a series of faults in the region associated with the Eburnean Orogeny (Figure 1) [e.g., *Feybesse and Milési*, 1994; *Debat et al.*, 2003], which were probably reactivated during the Pan-African Orogeny [*Ferré et al.*, 1996]. However, our shear wave splitting estimates are further in agreement with observations from the surface wave study of *Debayle et al.* [2005] down to depths of around 100–200 km. This, as well as the fact that we see no evidence of multiple layers of anisotropy, leads us to believe that the ENE-WSW trending fast directions are due to fossil anisotropic fabrics [e.g., *Silver and Chan*, 1991] throughout the crust and lithosphere resulting from Eburnean and Pan-African deformation.

Whether there is a contribution from anisotropy due to present-day mantle flow cannot be ascertained with certainty, a lack of depth constraint being an inherent problem of *SK(K)S* splitting analysis. However, the global mantle flow model of *Conrad and Behn* [2010] implies a small amount NE-SW trending (i.e., nearly parallel to measured fast directions and surface geology) horizontal mantle flow beneath the eastern WAC. Therefore, it may be that sublithospheric mantle anisotropy contributes to the measured shear wave splitting.

We interpret the prominent negative-polarity pulse arriving after the Moho *Ps* arrival to stem from an MLD at ~67 km depth (Figure 2). We consider the feature to be too shallow to be the LAB, as global surface wave tomography models [e.g., *Becker and Boschi*, 2002; *Debayle et al.*, 2005] infer a much deeper cratonic root (i.e., a thicker lithosphere) beneath SW Niger. Observations of MLDs are not uncommon in cratonic roots [e.g., *Snyder*, 2008; *Abt et al.*, 2010; *Miller and Eaton*, 2010; *Yuan and Romanowicz*, 2010; *Darbyshire et al.*, 2013; *Snyder et al.*, 2013; *Cooper and Miller*, 2014] and are, in fact, considered by some to be a ubiquitous feature in cratons [*Rychert and Shearer*, 2009]. However, the exact depths of these MLDs vary from craton to craton and may even vary significantly within a single craton [e.g., *Cooper and Miller*, 2014, and references therein], and thus, there are multiple theories on the nature and formation of MLDs.

Yuan and Romanowicz [2010] interpreted an MLD within the North American craton as a seismically sharp boundary between chemically depleted Archean lithosphere and an underlying thermal root that formed later. Similar observations were made by *Darbyshire et al.* [2013] for the Laurentian craton. Supporting evidence for a stratified cratonic lithosphere comes from thermobarometric analysis of xenoliths and xenocrysts [e.g., *Griffin et al.*, 2004].

In a recent study, *Cooper and Miller* [2014] elucidated the MLD structure in the WAC, primarily along its SW edge, using *S* RFs. The observed MLD depths vary from 75 to 160 km, and the authors tentatively note that there is a deepening of MLDs toward the center of the craton. This does not quite agree with our more shallow measurement of 67 km; however, the discrepancy might perhaps be due to the differing methodology. *Cooper and Miller* [2014] favor the view that these MLDs are relict structures from the craton's formation. We concur, but note that it is impossible to say how much of a deformational impact the subsequent Eburnean Orogeny or even the Pan-African Orogeny had. Further investigations and more data are required (e.g., to determine whether and how the MLD is dipping).

4.3. MTZ

Our results indicate that despite being below a thick craton, the MTZ appears to be thermally unperturbed. The apparent shallowing of the two bounding discontinuities, the "410" and the "660" (Figure 2), is due to the fast mantle velocities of the WAC. The thickness, however, is in good agreement with global average estimates [*Lawrence and Shearer*, 2006; *Tauzin et al.*, 2008]. As evident from their Clapeyron slopes, the 410 and the 660 vary in depth depending on given pressure-temperature conditions. The two Clapeyron slopes being opposite in sign means that the MTZ will be thicker in pervasively cold regions and thinner in hot regions [*Helffrich*, 2000]. Our observations match those of, e.g., *Flanagan and Shearer* [1998] and *Thompson et al.* [2011], in that we see no correlation between MTZ thickness and the continental lithosphere.

Although our measurements resemble but a pinprick in this large craton, we hope they add a valuable tessera to the mosaic that is our understanding of the nature of cratons. The study also shows the broader utility of IMS arrays for basic tectonic research.

References

Abt, D. L., K. M. Fischer, S. W. French, H. A. Ford, H. Yuan, and B. Romanowicz (2010), North American lithospheric discontinuity structure imaged by Ps and Sp receiver functions, *J. Geophys. Res.*, *115*, B09301, doi:10.1029/2009JB006914.

Becker, T. W., and L. Boschi (2002), A comparison of tomographic and geodynamic mantle models, *Geochem. Geophys. Geosyst*, *3*, 1003, doi:10.1029/2001GC000168.

Begg, G. C., W. L. Griffin, L. M. Natapov, S. Y. O'Reilly, S. P. Grand, C. J. O'Neill, J. M. A. Hronsky, Y. P. Djomani, C. J. Swain, T. Deen, and P. Bowden (2009), The lithospheric architecture of Africa: Seismic tomography, mantle petrology, and tectonic evolution, *Geosphere*, *5*, 23–50.

Braun, J. (2010), The many surface expressions of mantle dynamics, *Nat. Geosci.*, *3*, 825–833.

Christensen, N. I. (1996), Poisson's ratio and crustal seismology, *J. Geophys. Res*, *101*(B2), 3139–3156.

Conrad, C. P., and M. D. Behn (2010), Constraints on lithosphere net rotation and asthenospheric viscosity from global mantle flow models and seismic anisotropy, *Geochem. Geophys. Geosyst.*, *11*, Q05W05, doi:10.1029/2009GC002970.

Cooper, C. M, and M. S. Miller (2014), Craton formation: Internal structure inherited from closing of the early oceans, *Lithosphere*, *6*(1), 35–42.

Darbyshire, F. A., D. W. Eaton, and I. D. Bastow (2013), Seismic imaging of the lithosphere beneath Hudson Bay: Episodic growth of the Laurentian mantle keel, *Earth Planet Sci. Lett*, *373*, 179–193.

Debat, P., S. Nikiéma, A. Mercier, M. Lompo, D. Béziat, F. Bourges, M. Roddaz, S. Salvi, F. Tollon, and U. Wenmenga (2003), A new metamorphic constraint for the Eburnean orogeny from Paleoproterozoic formations of the Man shield (Aribinda and Tampelga countries, Burkina Faso), *Precambrian Res.*, *123*, 47–65.

Debayle, E., B. Kennett, and K. Priestley (2005), Global azimuthal seismic anisotropy and the unique plate-motion of Australia, *Nature*, *433*(7025), 509–512.

Durrheim, R. J., and W. D. Mooney (1991), Archean and Proterozoic crustal evolution: Evidence from crustal seismology, *Geology*, *19*(6), 606–609.

Ferré, E., J. Déléris, J. L. Bouchez, A. U. Lar, and J. J. Peucat (1996), The Pan-African reactivation of Eburnean and Archaean provinces in Nigeria: Structural and isotopic data, *J. Geol. Soc.*, *153*(5), 719–728.

Feybesse, J.-L., and J.-P. Milési (1994), The Archaean/Proterozoic contact zone in West Africa: A mountain belt of décollement thrusting and folding on a continental margin related to 2.1 Ga convergence of Archaean cratons?, *Earth Planet Sci. Lett*, *69*(1), 199–227.

Flanagan, M. P., and P. M. Shearer (1998), Global mapping of topography on transition zone velocity discontinuities by stacking SS precursors, *J. Geophys. Res*, *103*(B2), 2673–2692.

Frederiksen, A. W., S. W. Miong, F. A. Darbyshire, D. W. Eaton, S. Rondenay, and S. Sol (2007), Lithospheric variations across the Superior Province, Ontario, Canada: Evidence from tomography and shear wave splitting, *J. Geophys. Res.*, *112*, B07318, doi:10.1029/2006JB004861.

Griffin, W. L., S. Y. O'Reilly, B. J. Doyle, N. J. Pearson, H. Coppersmith, K. Kivi, V. Malkovets, and N. Pokhilenko (2004), Lithosphere mapping beneath the North American Plate, *Lithos*, *77*(1), 873–922.

Gurrola, H., J. B. Minster, and T. Owens (1994), The use of velocity spectrum for stacking receiver functions and imaging upper mantle discontinuities, *Geophys. J. Int.*, *117*, 427–440.

Helffrich, G. (2000), Topography of the transition zone seismic discontinuities, *Rev. Geophys.*, *38*(1), 141–158.

Helffrich, G. (2006), Extended-time multitaper frequency domain cross-correlation receiver-function estimation, *Bull. Seismol. Soc. Am.*, *96*(1), 344–347.

Helffrich, G., E. Asencio, J. Knapp, and T. Owens (2003), Transition zone structure in a tectonically inactive area: 410 and 660 km discontinuity properties under the northern North Sea, *Geophys. J. Int*, *155*, 193–199.

Hess, H. H. (1964), Seismic anisotropy in the uppermost mantle under oceans, *Nature*, *203*, 629–631.

Kay, I., S. Sol, J.-M. Kendall, C. Thomson, D. White, I. Asudeh, B. Roberts, and D. Francis (1999), Shear wave splitting observations in the Archean Craton of Western Superior, *Geophys. Res. Lett*, *26*(17), 2669–2672.

Kennett, B. L. N., E. R. Engdahl, and R. Buland (1995), Constraints on seismic velocities in the Earth from traveltimes, *Geophys. J. Int*, *122*, 108–124.

King, S. D., and J. Ritsema (2000), African hot spot volcanism: Small-scale convection in the upper mantle beneath cratons, *Science*, *290*, 1137–1140.

Langston, C. A. (1979), Structure under Mount Rainer, Washington, inferred from teleseismic body waves, *J. Geophys. Res*, *84*, 4749–4762.

Lawrence, J. F, and P. M. Shearer (2006), A global study of transition zone thickness using receiver functions, *J. Geophys. Res*, *111*, B06307, doi:10.1029/2005JB003973.

Mainprice, D., and A. Nicolas (1989), Development of shape and lattice preferred orientations: Application to the seismic anisotropy of the lower crust, *J. Struct. Geol.*, *11*(1/2), 175–189.

Miller, M. S., and D. W. Eaton (2010), Formation of cratonic mantle keels by arc accretion: Evidence from S receiver functions, *Geophys. Res. Lett*, *37*, L18305, doi:10.1029/2010GL044366.

Miller, M. S., A. A. Allam, T. W. Becker, J. F. Di Leo, and J. Wookey (2013), Constraints on the tectonic evolution of the westernmost Mediterranean and northwestern Africa from shear wave splitting analysis, *Earth Planet Sci. Lett.*, *375*, 234–243.

Nicolas, A., and N. I. Christensen (1987), Formation of anisotropy in upper mantle peridotites—A review, in *Composition, Structure and Dynamics of the Lithosphere-Asthenosphere System*, vol. 16, edited by K. Fuchs and C. Froidevaux, pp. 111–123, AGU, Washingon, D. C.

Rondenay, S., M. G. Bostock, T. M. Hearn, D. J. White, and R. M. Ellis (2000), Lithospheric assembly and modification of the SE Canadian Shield: Abitibi-Grenville teleseismic experiment, *J. Geophys. Res*, *105*, 13,735–13,754.

Rychert, C. A., and P. M. Shearer (2009), A global view of the lithosphere-asthenosphere boundary, *Science*, *324*, 495–498.

Silver, P. G., and W. W. Chan (1991), Shear wave splitting and subcontinental mantle deformation, *J. Geophys. Res*, *96*, 16,429–16,454.

Snyder, D. B. (2008), Stacked uppermost mantle layers within the Slave craton of NW Canada as defined by anisotropic seismic discontinuities, *Tectonics*, *27*, TC4006, doi:10.1029/2007TC002132.

Snyder, D. B., R. G. Berman, J.-M. Kendall, and M. Sanborn-Barrie (2013), Seismic anisotropy and mantle structure of the Rae craton, central Canada, from joint interpretation of SKS splitting and receiver functions, *Precambrian Res.*, *232*, 189–208, doi:10.1016/j.precamres.2012.03.003.

Tauzin, B., E. Debayle, and G. Wittlinger (2008), The mantle transition zone as seen by global Pds phases: No clear evidence for a thin transition zone beneath hotspots, *J. Geophys. Res*, *113*, B08309, doi:10.1029/2007JB005364.

Thompson, D. A., I. D. Bastow, G. Helffrich, J.-M. Kendall, J. Wookey, D. B. Snyder, and D. W. Eaton (2010), Precambrian crustal evolution: Seismic constraints from the Canadian Shield, *Earth Planet Sci. Lett.*, *297*(3), 655–666.

Thompson, D. A., G. Helffrich, I. D. Bastow, J.-M. Kendall, J. Wookey, D. W. Eaton, and D. B. Snyder (2011), Implications of a simple mantle transition zone beneath cratonic North America, *Earth Planet Sci. Lett.*, *312*(1), 28–36.

Van Hinsbergen, D. J., S. J. Buiter, T. H. Torsvik, C. Gaina, and S. J. Webb (2011), The formation and evolution of Africa from the Archaean to present: Introduction, in *The Formation and Evolution of Africa: A Synopsis of 3.8 Ga of Earth History*, edited by D. J. J. Van Hinsbergen et al., *Geol. Soc. London Spec. Publ.*, *357*, 1–8.

Wolfe, C. J., and P. G. Silver (1998), Seismic anisotropy of oceanic upper mantle: Shear wave splitting methodologies and observations, *J. Geophys. Res*, *103*(B1), 749–771.

Wüstefeld, A., O. Al-Harrasi, J. P. Verdon, J. Wookey, and J.-M. Kendall (2010), A strategy for automated analysis of passive microseismic data to image seismic anisotropy and fracture characteristics, *Geophys. Prospect.*, *58*, 755–773.

Yuan, H., and B. Romanowicz (2010), Lithospheric layering in the North American craton, *Nature*, *466*, 1063–1069, doi:10.1038/nature09332.

Zhu, L., and H. Kanamori (2000), Moho depth variation in southern California from teleseismic receiver functions, *J. Geophys. Res.*, *105*(B2), 2969–2980.

DI LEO ET AL.   1700